REPORT DOCUMENTATION PAGE

Form Approved OMB No. 0704-0188

1. REPORT DATE *(DD-MM-YYYY)*	2. REPORT TYPE	3. DATES COVERED *(From - To)*
07-12-2005	Final Contractor Report	June 2004 - June 2005

4. TITLE AND SUBTITLE
Large-Bandwidth, Phase-Locked Measurements for High-Speed Flow Experiments with Controlled Disturbance Inputs

5a. CONTRACT NUMBER
FA95550-04-1-0397

5b. GRANT NUMBER
N/A

5c. PROGRAM ELEMENT NUMBER
N/A

6. AUTHOR(S)
Chokani, Ndaona

5d. PROJECT NUMBER
N/A

5e. TASK NUMBER
N/A

5f. WORK UNIT NUMBER
N/A

7. PERFORMING ORGANIZATION NAME(S) AND ADDRESS(ES)
Duke University
Office of Sponsored Programs
705 Broad Street, Box 90941
Durham, NC 27708-0491

8. PERFORMING ORGANIZATION REPORT NUMBER
N/A

9. SPONSORING / MONITORING AGENCY NAME(S) AND ADDRESS(ES)
AFOSR/NA.
AF Office of Scientific Research
875 North Randolph Street
Arlington, VA 22203
Dr John Schmisseur

10. SPONSOR/MONITOR'S ACRONYM(S)
AFOSR

11. SPONSOR/MONITOR'S REPORT NUMBER(S)
N/A

12. DISTRIBUTION / AVAILABILITY STATEMENT
Approved for Public Release. Distribution unlimited. -A

AFRL-SR-AR-TR-06-0107

13. SUPPLEMENTARY NOTES
N/A

14. ABSTRACT
The purpose of the present work is to develop an experimental apparatus that will enable us to accurately detect, and then measure, the phase-locked interactions that occur in high-speed flows. In particular, we examine the structure of the shockwave / boundary layer interaction induced by an unswept compression ramp flow in the Supersonic Low Disturbance Wind Tunnel at the NASA Langley Research Center. SLDT has a unique capability for generating a very low disturbance environment with a free-stream noise level that is at least an order of magnitude lower than in conventional facilities. This low level of natural free-stream disturbances is advantageous for the generation of controlled free-stream disturbances with an acoustic generator. Measurement of the fluctuating density gradients are performed using a focusing schlieren deflectometer, which is a promising technique for large-bandwidth, phase-locked measurements in high-speed flows.

15. SUBJECT TERMS
High-Speed Flows, Measurement Techniques.

16. SECURITY CLASSIFICATION OF:			17. LIMITATION OF ABSTRACT	18. NUMBER OF PAGES	19a. NAME OF RESPONSIBLE PERSON
a. REPORT	b. ABSTRACT	c. THIS PAGE			Ndaona Chokani
Unclassified	Unclassified	Unclassified	None	25	19b. TELEPHONE NUMBER *(include area code)* (919) 660-5310

Table of contents

Acknowldegments

The author is grateful to Julien Weiss for preparing the report. Dr. Weiss served as a post-doctoral research assistant under the companion AFOSR grant FA9550-05-1-0178 entitled "Quiet-Tunnel Experiments Of Shockwave/Transitional & Turbulent Boundary Layer Interactions On Compression Ramps"

The views and conclusions contained herein are those of the author and should not be interpreted as necessarily representing the official policies or endorsements, either expressed or implied, of the Air Force Office of Scientific Research or the U.S. Government.

1.0 Introduction

The drag on high-speed flight, the performance and operability of the engines and the requirements of the thermal protection system of the vehicle are directly impacted by boundary layer transition and shockwave / boundary layer interaction. Despite the significant progress that has been made over the last decade, the prediction of shockwave / boundary layer interaction (SBLI) using numerical methods is still far from satisfactory. For example, although the mean pressure distributions can be predicted quite well using Reynolds averaged Navier Stokes (RANS) computations, other parameters such as skin friction, heat transfer, and fluctuating thermo-mechanical loads are not accurately predicted.

One of the reasons for the poor RANS predictions is the inherent unsteadiness of SBLI (Dolling, 1998). Indeed, a number of experimental studies have shown that the shock wave structure in different types of SBLIs is characterized by large-scale random shock oscillations. This motion is in turn responsible for the large fluctuating pressure loads at the wall. However Dolling (2001) indicates that the mechanisms driving the shock oscillations are not well understood. Dynamic wall pressure measurements in shock-induced separated flows have shown that the interaction is characterized by an intermittent zone in which the fluctuating wall pressure signal has contributions from three different flow components: the incoming turbulent boundary layer, the separated flow downstream of the shock, and the rapid rises and falls in pressure associated with the shock foot. This latter motion produces the largest contribution to the total RMS of the signal. The frequency of the shock foot motion appears to be at least an order of magnitude lower than the boundary layer's characteristic frequency U/δ, where U is the free stream velocity and δ is the boundary layer thickness (Dolling, 2001). This relatively low frequency motion of the shock foot is observed in compression ramp, blunt fin, and cylinder-induced interactions. Andreopoulos and Muck (1987) conducted experiments on a Mach 3 compression ramp flow, and suggested that the frequency of the shock motion scales with the bursting frequency of the incoming turbulent boundary layer. This observation was, however, not confirmed in the experiments of Thomas et al (1994) who specifically addressed this question. Erengil and Dolling (1991) showed that there is a correlation between the wall pressure fluctuations beneath the incoming boundary layer and the velocity of the separation shock foot; they therefore inferred that the small-scale motion of the shock is caused by its response to the passage of turbulent fluctuations through the interaction, whereas the large-scale motion is a result of the shock's displacement due to expansion and contraction of the separation bubble. Ünalmis and Dolling (1998) studied the relationship between the separation shock motion and the Pitot pressure in the upstream turbulent boundary layer, and Beresh et al (2002) used particle image velocimetry to correlate the velocity fluctuations in the incoming boundary layer with the fluctuating wall pressure. Though all these experiments shed some light on the possible mechanisms that play a role in the shock motion, there is still no comprehensive

explanation of the physical causes of the unsteadiness. In particular, it has been speculated that that the shock unsteadiness may be facility induced (Hou et al, 2004).

The purpose of the present work is to develop an experimental apparatus that will enable us to accurately detect, and then measure, the phase-locked interactions that occur in high-speed flows. In particular, we examine the structure of the SBLI induced by an unswept compression ramp flow in the Supersonic Low Disturbance Wind Tunnel (SLDT) at the NASA Langley Research Center. SLDT has a unique capability for generating a very low disturbance environment with a free-stream noise level that is at least an order of magnitude lower than in conventional facilities. This low level of natural free-stream disturbances is advantageous for the generation of controlled free-stream disturbances with an acoustic generator. Measurement of the fluctuating density gradients are performed using a focusing schlieren deflectometer, which is a promising technique for large-bandwidth, phase-locked measurements in high-speed flows.

2.0 Facility

Experiments were performed in the Mach 3.5 SLDT at the NASA Langley Research Center. In this tunnel, the nozzle boundary layer can be removed by bleed slots located just upstream of the nozzle throat. The boundary layer that develops downstream of the nozzle throat is therefore initially laminar. Since most of the free stream disturbances are fluctuating Mach waves that are radiated from the turbulent boundary layer, this results in a portion of the test section – the so-called "quiet test core" – which is free from acoustic disturbances (Chen et al, 1988). The level of disturbances in the quiet test core is typically one order of magnitude lower than in the portion contaminated by acoustic radiation. The tunnel can also be run in a "noisy" mode by closing the bleed slots. In this case, the boundary layer on the nozzle is turbulent from the throat and the disturbance levels in the test section are similar to those in a conventional facility. Therefore, operation of the tunnel with bleed valves open (BVO) or closed (BVC) (i.e. quiet or noisy conditions) readily provides a means to examine the effect of free-stream disturbances on SBLI. A schematic picture of SLDT's test section is shown in figure 1. The free-stream disturbances on the centerline of the tunnel were measured using a hot-wire probe. The streamwise distributions of static pressure fluctuations, derived from the hot-wire measurements, for BVO ("quiet" flow) and BVC ("noisy" flow) conditions are shown in Fig. 2 for a stagnation pressure of p_0=25psi.

The model was a 11.5*in* long × 7*in* wide (292mm × 178mm) flat plate that was mounted in the center of the test section. A 24-degrees compression ramp was mounted on the rear portion of the plate to generate a separated SBLI. The flat plate was instrumented with 4 Entran EPIH 113-50psi miniature dynamic pressure transducers mounted upstream of the compression ramp. Unfortunately, hardware problems were encountered during the course of the experiments and no data could be gathered with these transducers. Both the wind tunnel model and the pressure transducers were purchased under this DURIP grant (FA9550-04-1-0397).

3.0 Focusing Schlieren Deflectometer

A focusing schlieren deflectometer was designed to enable large-bandwidth, phase-locked measurement of unsteady density gradients. Focusing schlieren deflectometry is the combination of an optical deflectometer (basically a quantitative schlieren system) with a focusing schlieren setup. This technique has been developed and validated by Garg and Settles (1998) in a supersonic turbulent boundary layer. In essence, it consists in the measurement of light intensity fluctuations at discrete points in a real time schlieren image of the flow field. Fiber optic cables in combination with photomultiplier tubes (PMT) as the light detectors provide a high spatial resolution with virtually unlimited frequency response. In contrast to the standard schlieren approach, where the measured quantity reflects an integral of flow properties along the entire path of a given light ray, focusing schlieren deflectometry allows measurements in a narrow "slice" of the flow, the so-called plane of best focus. This property is very valuable for the investigation of shock unsteadiness in SBLI since it has been shown that the shock motion is not completely two-dimensional.

Most of the components that were used in the design of the focusing schlieren deflectometer were purchased under this DURIP grant (FA9550-04-1-0397).

3.1 Design of the Focusing Schlieren System

The most important building block of the focusing schlieren deflectometer is the focusing schlieren system itself. The present focusing schlieren system closely follows the design of Weinstein (1993) but its characteristic details have been driven by the specific needs of the experiments as well as the geometry of the wind tunnel. The most critical constraint is to achieve a small depth of field without relying on a large and very expensive imaging lens. It is also important to be able to take microsecond exposure photographs of the flowfield. On the other hand, the size of the field of view does not need to be very large.

A schematic description of the system is given in figure 3. The illumination optics consist in a short duration flash lamp (Spectralite 919), two collimating lenses (L1, L2), a diffuser, a Fresnel lens (F1), and the source grid. The goal of the two collimating lenses is to create a light spot of specific diameter at the diffuser. The Fresnel lens F1 then focuses this light source on the imaging lens L3, thus acting as a light condenser. The diffuser consists in two sheets of holographic diffusing material with a high transmittance and a spreading angle of approximately 10 degrees.

The imaging optics consist in the imaging lens L3, the cut-off grid, and the viewing screen. The cut-off grid is a photographic negative image of the source grid that can be translated in the x direction to vary the schlieren sensitivity. The position of the viewing

screen determines the plane of best focus in the flow field. The viewing screen consists in a large sheet of holographic diffusing material.

The schlieren image is recorded by a CCD camera after passing through the Fresnel lens F2 and the camera lens L4. The Fresnel lens condenses the light on the aperture of the camera lens L4, which then images a portion of the viewing screen on the CCD chip.

The dimensions of the system are given in table 1 and the characteristics of the lenses are given in table 2.

L	1270 mm
l	635 mm
L'	584 mm
l'	1081 mm

Table 1 : main dimensions

Lens	Focal lenght	Aperture
L1	50 mm	50 mm
L2	100 mm	50 mm
L3	400 mm	75 mm
L4	12.5 mm	8.9 mm
F1	150 mm	150 mm
F2	100 mm	200 mm

Table 2 : lens dimensions

The schlieren image is recorded with a Pulnix TM-1040 video camera with a CCD chip of 9.1 mm x 9.2 mm. The source grid is a square of 150 mm x 150 mm with vertical black & transparent stripes of 1mm width obtained using a photoplotter. To expose the cut-off grid, the illumination optics was replaced by a standard 15W light bulb operated at a line voltage of 25 Volts. The grid was exposed for 8 seconds on a sheet of Kodak Technical Pan 4''x 5'' film and developed for 2 minutes using the Kodak D-19 developer at 22°C. Particular attention was taken to operate in total darkness during the exposure and development of the cut-off grid.

Figures 4, 5, and 6 show pictures of the actual system.

3.2 Performance of the Focusing Schlieren System

The performance of the system can be computed using the formulae derived by Weinstein (1993).

Assuming that the smallest change in brightness that can be detected is 10%, the sensitivity of the focusing schlieren system is given by:

$$\varepsilon_{\min} = 20626\frac{aL}{L'(L-l)} \text{ arcsec},$$

where a is the half height of the light source image in the cut-off plane. It should be noted that the 10% criterion was developed for pictures taken on film paper. Modern digital imaging actually allows detection of much smaller changes in brightness so that the corresponding sensitivity is higher.

The resolution of features in the test section is given by:

$$w = \frac{2(l'-L')\lambda}{mb},$$

where λ is the wavelength of the light, m is the object magnification, and b is the clear height of the cut-off gridlines.

The primary parameter that determines the depth of field is the quantity $R=l/A$, which is the ratio of the distance between the object and imaging lens and the lens aperture. The depth of field of an imaging system depends on the size of an acceptable blur caused by defocusing. If B is the size of the blur, then the depth of field is given by $2RB$ (Smith, 2000). For a focusing schlieren system, Weinstein (1993) defines the depth of unsharp focus DU by choosing a blur size of 2mm, so that:

$DU = 4R$ mm.

The quantity R is also related to the number of source gridlines that actually form an image of the object. If the source grid has n source lines per millimeter, the number N of gridlines that blend to form an image is given by:

$$N = \frac{(L-l)n}{R}.$$

The theoretical field of view is given by:

$$F_{th} = A + \frac{l(D-A)}{L},$$

where D is the size of the source grid. With D=150mm, this corresponds to a theoretical field of view of 112 mm.

In the present case, however, the camera lens also limits the field of view. Indeed, the practical field of view F_{pr} is given by the largest portion of the viewing screen that can be imaged by the camera lens. The camera lens is mounted 110 mm behind the viewing screen, so that its magnification is 0.13. If the size of the CCD chip is 9mm, this gives a maximum image size of 70mm at the viewing screen, and a corresponding field of view of 41 mm in the object plane. This small field of view is actually well suited for the shockwave – boundary layer experiments for which the schlieren system was designed.

Table 3 summarizes the characteristics of the present system.

Quantity	Unit	Value
a	mm	0.23
b	mm	0.46
ε_{min}	arcsec	16.2
λ	μm	0.5
m	-	1.70
w	mm	0.64
R	-	8.47
DU	mm	34
n	1/mm	0.5
N	-	37
F_{pr}	mm	41

The depth of field of the focusing schlieren system was tested by taking pictures of a low velocity helium jet. The images that are focused on different planes in the field are shown in figures 7 through 10. The inner diameter of the jet orifice is 4mm and the flash duration is approximately 2 microseconds. The fine turbulent structures of the jet can be observed when the jet is in focus. When the jet is moved 25.4mm out of focus, only the large-scale details are visible. The picture becomes significantly blurred when jet is positioned 50mm away of the plane of best focus.

It is clear from these images that the focusing properties of the system depend on the length scale of the disturbances. The small-scale structures are still barely visible when the jet is 25.4mm out of focus and completely disappear from the image at larger distances. The large-scale shape of the jet, however, is still visible at 76.2mm.

3.3 Performance of the Focusing Schlieren Deflectometer

To use the focusing schlieren system as a deflectometer, a fiber optic sensor was placed on the image plane and the light intensity was recorded using a photomultiplier tube (PMT). The PMT used in this work was a Hamamatsu HC124-01 equipped with a built-in amplifier having an overall cut-off frequency of approximately 20kHz. It should be noted that this particular PMT was used to verify the capabilities of the system and not to actually perform the measurements in SLDT. Measurements of fluctuating density gradients in a supersonic flow would require a PMT with a higher bandwidth.

To test the system, measurements of density gradient fluctuations were performed in a second turbulent helium jet that issued into quiescent air. Fig. 11 shows a schlieren image of the helium jet. In this case, the jet is mounted horizontally. The diameter of the nozzle exit is 2mm and the black cross marks the position of the fiber optic pickup sensor. The sensor, which has a diameter of 0.140mm, is positioned along the jet centerline, 25mm downstream of the nozzle exit. At this location, the mean velocity on the jet centerline is approximately U=20m/s. The source and cut-off grids are mounted vertically (y-direction), so that density gradients along the jet axis can be detected. The voltages are directly recorded on an oscilloscope and no attempt is made to relate the voltage to the light intensity. Measurements were first made with the plane of best focus along the centerline of the jet; the jet was then translated away from the plane of best focus for subsequent measurements. This provided a way to test the integration properties of the deflectometer.

The power spectral densities (PSD) of the measured signals are shown in Fig. 12 for different positions of the jet. The sampling frequency is 50kHz and the PSD is computed by averaging 24 blocks of 2048 samples and using a Hanning window. The peak at 120Hz is due to the AC fluctuations in the regular frosted light bulb that is used as the light source. Above this frequency, the PSD levels decrease with increasing frequency, which is indicative of the turbulent character of the jet flow. Also shown is the PSD of the background noise; this signal is obtained by measuring the output of the PMT signal when the flow is turned off. The strongest signal was obtained when the jet's centerline was located in the plane of best focus. As the displacement of the jet centerline was increased from the plane of best focus, the PSD levels decreased. A close examination of Fig. 12 reveals that the attenuation is a function of the frequency: that is, the attenuation is less at lower frequencies than at higher frequencies. This can also be inferred from the images presented above. Namely, for a given convective velocity, a low frequency implies a disturbance of large length scale, whereas a large frequency suggests a disturbance of small length scale. Thus, as z is increased, the relative intensity of a small scale (large frequency) disturbance is more attenuated than that of a large scale (low frequency) disturbance.

Fig. 13 shows the variation of the relative intensity of the measured signal as a function of z. The root mean square (RMS) of the measured signal is computed for two frequency bins centered at f=1kHz and f=10kHz. Each frequency bin has a width of Δf=1kHz and the RMS values are normalized by the corresponding RMS value in the plane of best focus (z=0). It is evident that the 10kHz disturbances are more attenuated than the 1kHz. A practical consequence of these results is that the measured spectrum of a turbulent flow depends on the position of the fluctuating field along the optical axis, as demonstrated in Fig. 12. This applies to the amplitude as well as the shape of the spectrum.

4.0 Shockwave – Boundary Layer Experiment

The focusing schlieren system described in the last section was used to investigate the effect of free-stream noise on the structure of supersonic compression ramp flows. To this end, the focusing schlieren system was mounted across the test section of SLDT and images of the separation shock were taken for both bleed valves closed (BVC) and bleed valves open (BVO) conditions. The light source is a microsecond spark and the flow can therefore be considered as "frozen". All images are taken with the cut-off grid closed at 50%.

The schlieren images are shown in figures 14 through 21. They were taken for both BVC and BVO at four values of the stagnation pressure: p_0 = 25, 35, 50, and 75 psi.

For BVC conditions, the ramp-induced compression results in a shock wave that is visible upstream of the ramp for all values of the stagnation pressure. For BVO conditions, the compression region is not well defined at 25 psi and 35 psi. This is most likely due to a laminar incoming boundary layer, which results in a very large separation region. At p_0 = 50 psi and p_0 = 75 psi, the separation shock is visible for both BVO and BVC conditions. However, the shock is located more downstream for the BVO case. This is attributed to a thinner boundary layer in the BVO case. Indeed, laminar-turbulent transition occurs more downstream when the free-stream disturbance level is low, this results in a thinner boundary layer at the start of the interaction, and a corresponding smaller global interaction scale.

Unfortunately, the position of the separation shock is not seen very clearly in the images. Instead of a sharp line, the separation shock is seen as a broad dark region located upstream of the ramp. This is clearly seen in figure 22, which shows a zoomed-in view of this region for 35psi BVC. This effect is attributed to the spanwise variation of the separation region. Indeed, it is known that the separation shock is never fully two-dimensional. This spanwise "rippling" usually results in a layered appearance of the shock foot in conventional schlieren images (Smits & Dussauge, 1996). In the present investigation, the focusing schlieren technique was chosen to avoid this effect. Unfortunately, the focusing capabilities of the present system are not sufficient to visualize the separation shock sharply enough. In contrast to conventional schlieren systems, the image of the focusing schlieren is weighted towards the plate centerline. The

light rays, however, are influenced by density gradients over the whole span of the plate so that regions away from the plate centerline also contribute – although less strongly – to the final image.

5.0 Concluding remarks

An innovative method for large-bandwidth, phase-locked measurements for high-speed flow experiments with controlled disturbance inputs is presented in this report. Measurements of the fluctuating density gradients are performed with a focusing schlieren deflectometer. In contrast to the standard schlieren approach, where the measured quantity reflects an integral of flow properties along the entire path of a given light ray, focusing schlieren deflectometry allows measurements in a narrow "slice" of the flow, the so-called plane of best focus. This characteristic is well suited for the investigation of shock unsteadiness in shockwave / boundary layer interactions since it has been shown that the shock motion is not completely two-dimensional. In particular, the focusing schlieren deflectometer can be advantageously combined with a lock-in amplifier and other advanced signal processing units to perform accurate large-bandwidth, phase-locked measurements in high-speed flow experiments.

The integration properties of the focusing schlieren deflectometer are investigated experimentally. It is shown that the depth of field of the system depends on the disturbance length scale in the flow: the signal produced by out-of-focus disturbances is larger for large-scale disturbances than for small-scale disturbances. Thus, the measured spectrum of a turbulent flow depends on the position of the fluctuating field along the optical axis.

The structure of the SBLI induced by an unswept compression ramp flow is then investigated in the Supersonic Low Disturbance Wind Tunnel at the NASA Langley Research Center. SLDT has a unique capability for generating a very low disturbance environment with a free-stream noise level that is at least an order of magnitude lower than in conventional facilities.

Focusing schlieren images of shockwave / boundary layer interactions in SLDT reveal that the structure of the interaction depends on the level of free-stream disturbances in the flow. However, the focusing capabilities of the present system are not sufficient to visualize the separation shock sharply enough. Thus, more development work is needed to improve the capabilities of the schlieren system and to develop a deflectometer. When this is done, the system will be ready to be combined with a lock-in amplifier and other advanced signal processing units to perform accurate large-bandwidth, phase-locked measurements of shockwave / boundary layer interactions and other high-speed flow experiments of interest for the Air Force's research program.

6.0 References

Andreopoulos, J., Muck, K.C. "Some New Aspects of the Shock-Wave/Boundary Layer Interaction in Compression Ramp Flows", *J. Fluid. Mech.* 180, pp. 405-428, 1987

Beresh, S.J., Clemens, N.T., Dolling, D.S., "Relationship Between Upstream Turbulent Boundary-Layer Velocity Fluctuations and Separation Shock Unsteadiness", *AIAA J.* 40 (12), pp. 2412-2422, 2002

Chen, F.-J., Malik, M.R., Beckwith, I.E. "Comparison of Boundary Layer Transition on a Cone and Flat Plate at Mach 3.5", AIAA 88-0411, 1988.

Dolling, D.S. "High-Speed Turbulent Separated Flows : Consistency of Mathematical Models and Flow Physics", *AIAA J.* 36 (5), pp.725-732, 1998

Dolling, D.S. "Fifty Years of Shock-Wave/Boundary-Layer Interaction Research: What Next?", *AIAA J.* 39 (8), pp.1517-1531, 2001

Erengil, M.E., Dolling, D.S. "Correlation of Separation Shock Motion with Pressure Fluctuations in the Incoming Boundary Layer", *AIAA J.* 29 (11), pp. 1868-1877, 1991

Garg, S. and Settles, G.S., "Measurements of a Supersonic Turbulent Boundary Layer by Focusing Schlieren Deflectometry", *Exp. Fluids* 25(3) , pp.254-264, 1998

Hou, Y.X., Ünalmis, Ö.H., Bueno, P.C., Clemens, N.T., Dolling, D.S. "Effects of Boundary-Layer Velocity Fluctuations on Unsteadiness of Blunt-Fin Interactions", *AIAA J.* 42 (12), pp. 2615-2618, 1991

Smith, W.J. *Modern Optical Engineering*, McGraw-Hill, 2000

Smits, A.J., Dussauge, J.P. *Turbulent Shear Layers in Supersonic Flows*, AIP Press, 1996

Thomas, F.O., Putnam, C.M., Chu, H.C. "On the Mechanism of Unsteady Shock Oscillation in Shock Wave / Turbulent Boundary Layer Interactions", *Exp. Fluids* 18, pp.69-81, 1994

Ünalmis, Ö.H., Dolling, D.S. "Experimental Study of Causes of Unsteadiness of Shock-Induced Turbulent Separation", *AIAA J.* 36 (3), pp. 371-378, 1998

Weinstein, L.M., "Large-Field High-Brightness Focusing Schlieren System", *AIAA Journal*, Vol. 31, No. 7, 1993, pp. 1250-1255.

7.0 Figures

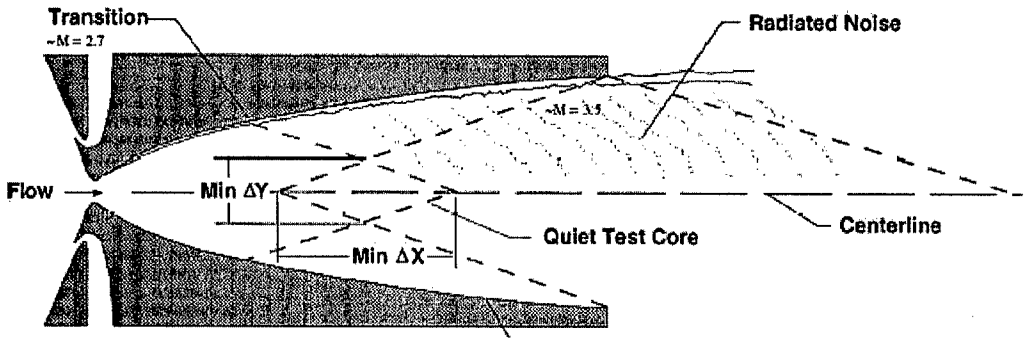

Figure 1 : Test section of SLDT (schematic)

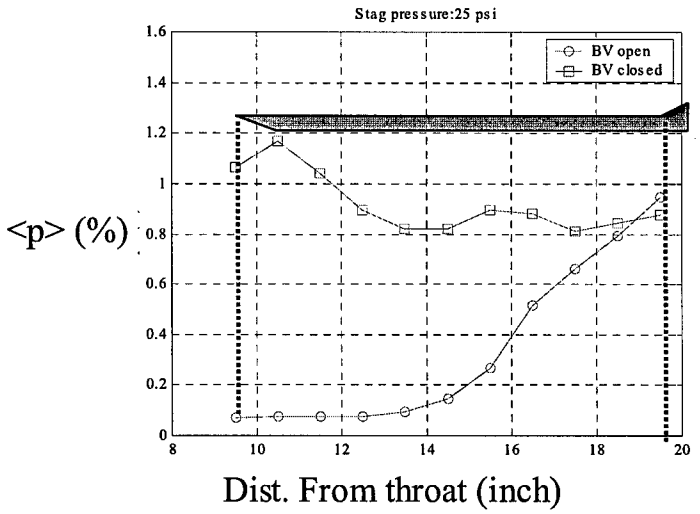

Figure 2 : Static pressure fluctuations along centerline of SLDT, p_0 = 25psi

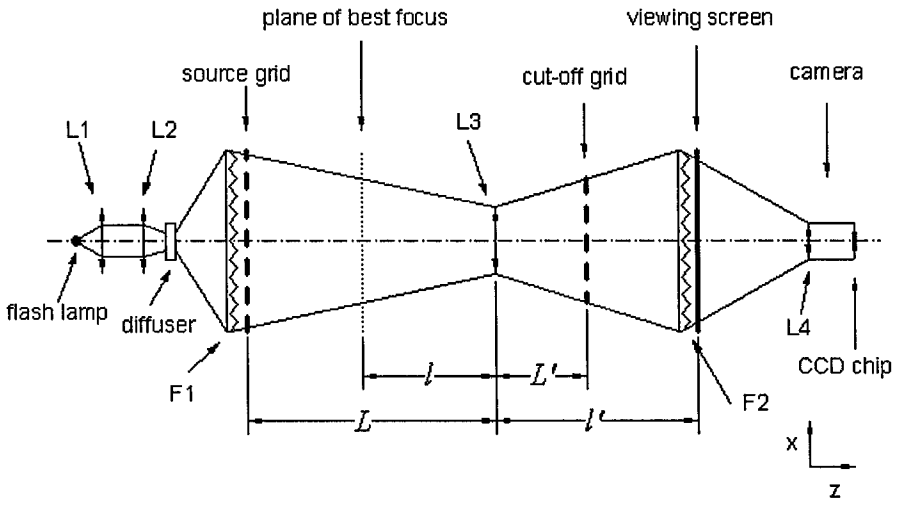

Figure 3 : Focusing schlieren setup (schematic)

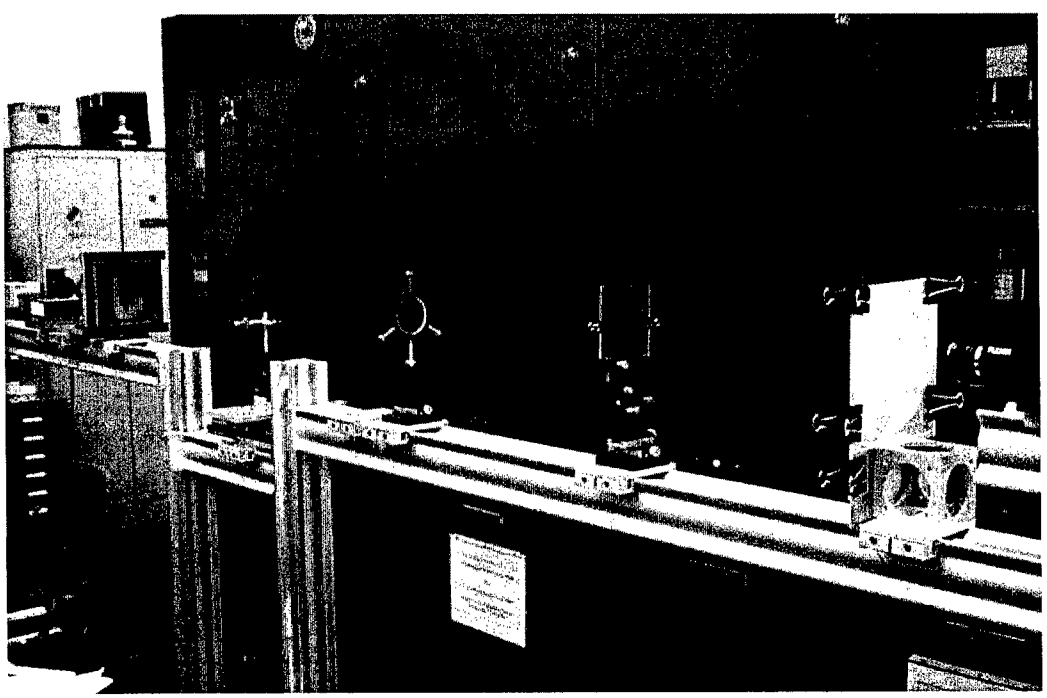

Figure 4 : Photograph of focusing shlieren setup

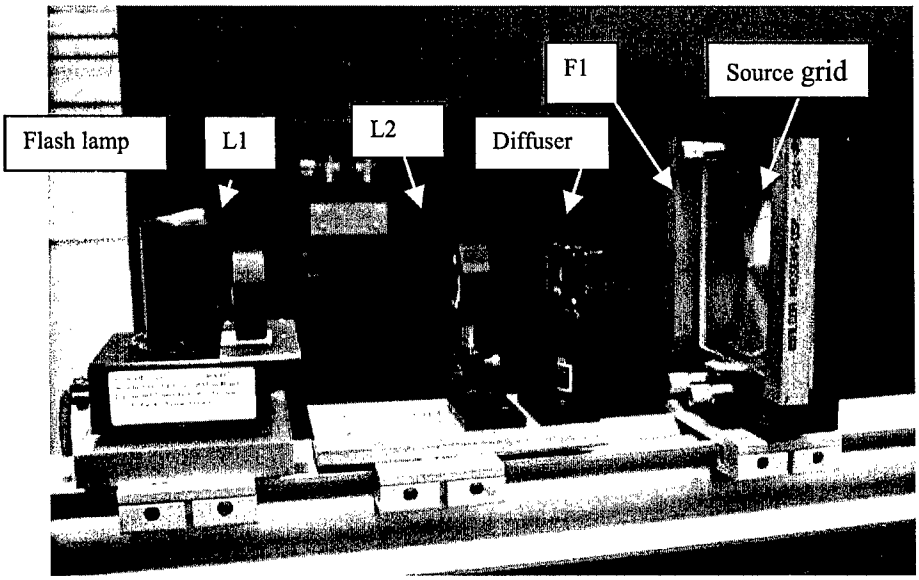

Figure 5 : detail of illumination optics

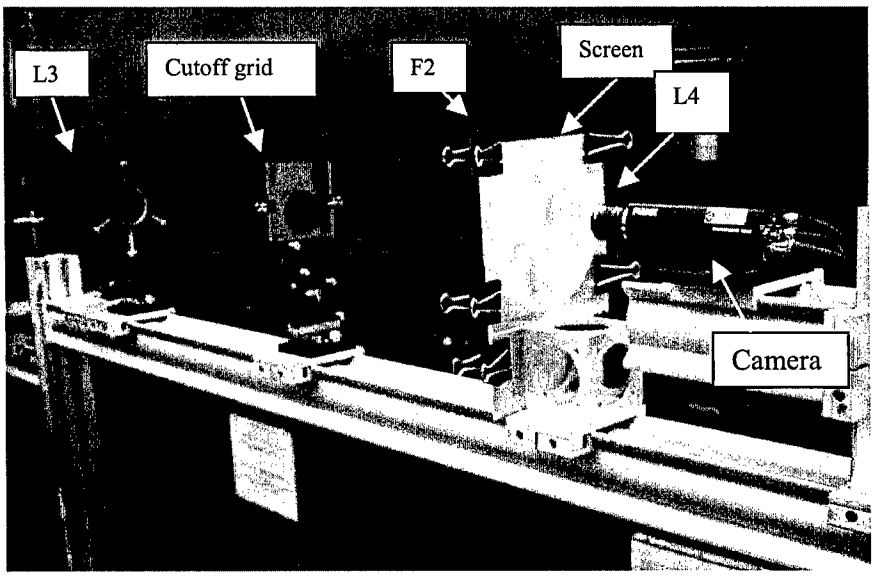

Figure 6 : Detail of imaging optics

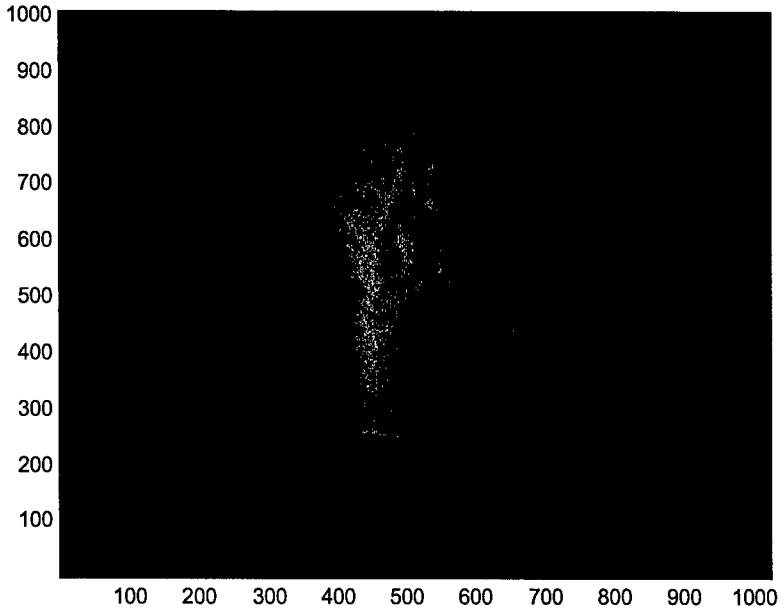

Figure 7 : helium jet in focus

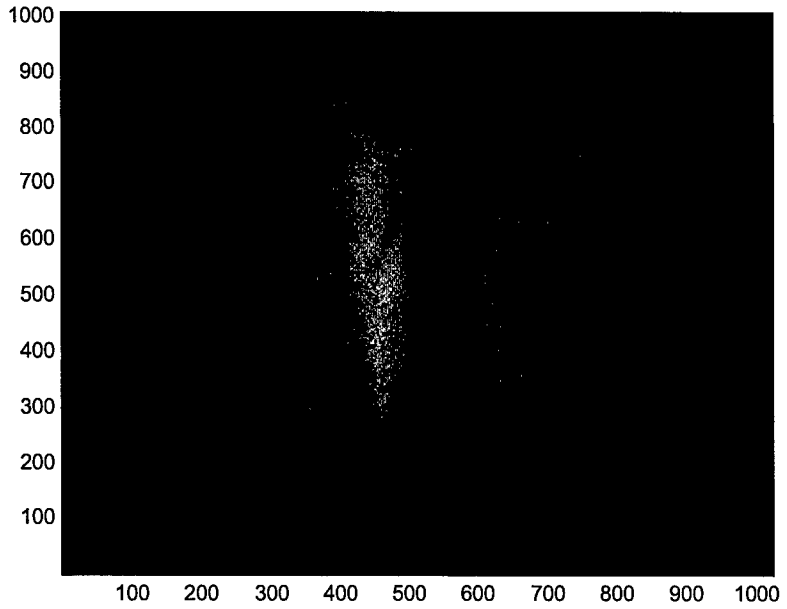

Figure 8 : helium jet 25.4 mm out of focus

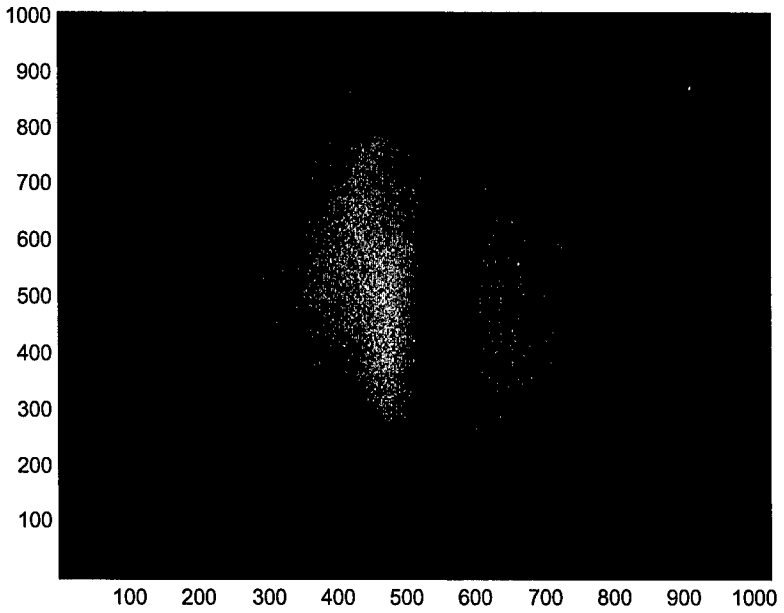

Figure 9 : helium jet 50.8 mm out of focus

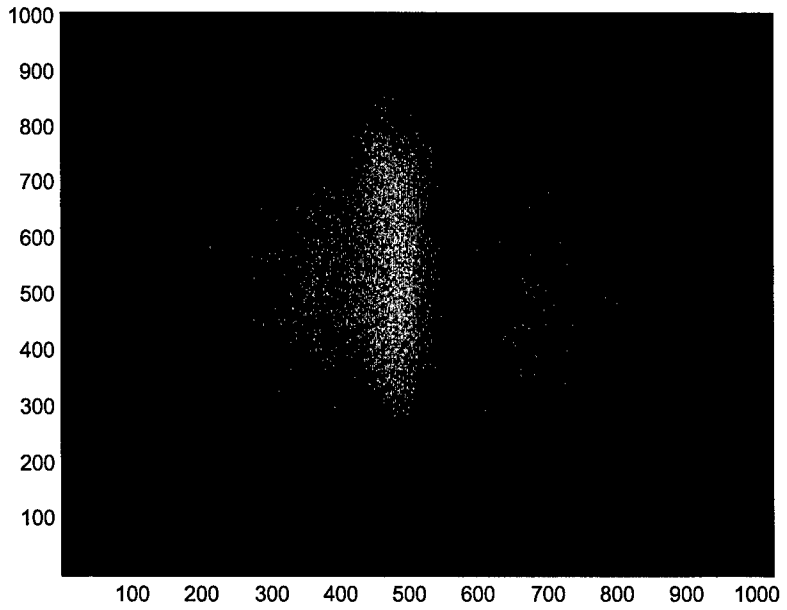

Figure 10 : helium jet 76.2 mm out of focus

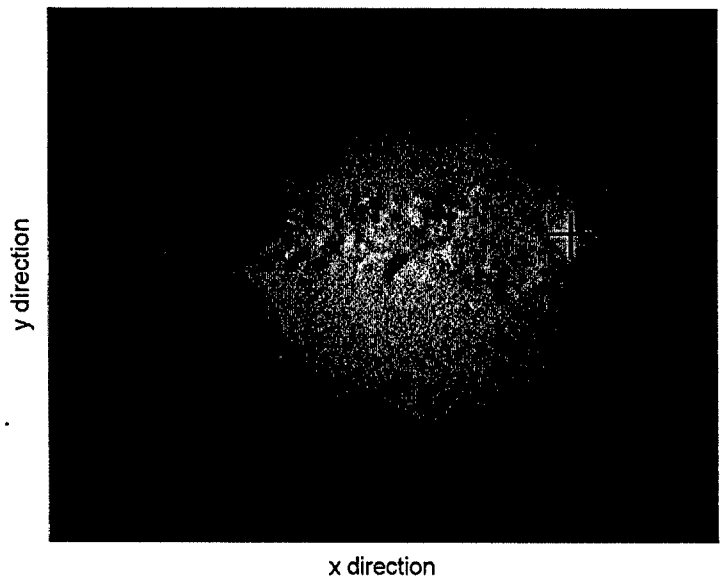

Figure 11 : Schlieren image of turbulent helium jet. The black cross marks the position of the fiber optic sensor.

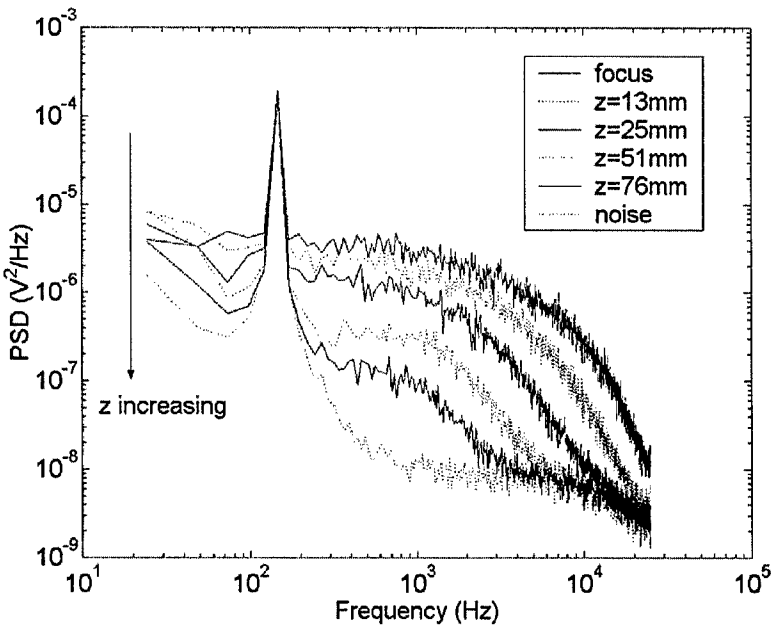

Figure 12 : PSD of measured signals

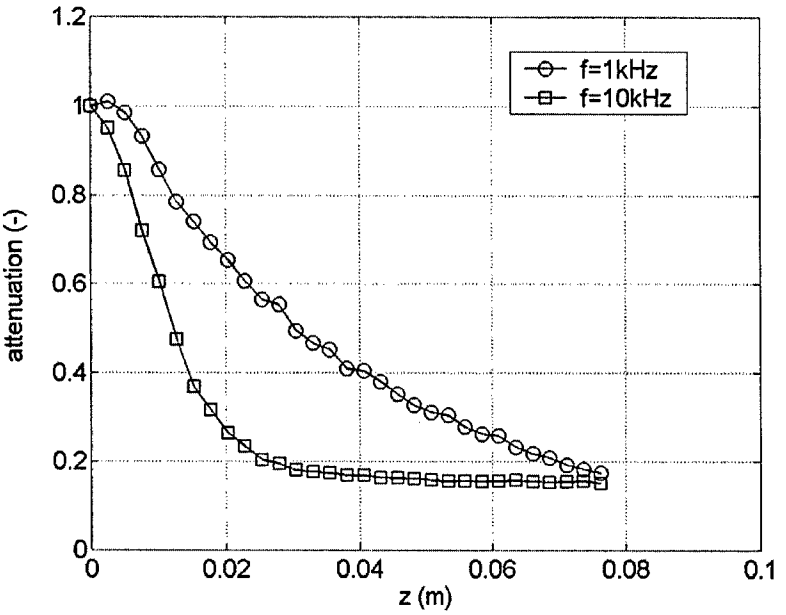

Figure 13 : Attenuation of signal RMS as a function of z-position

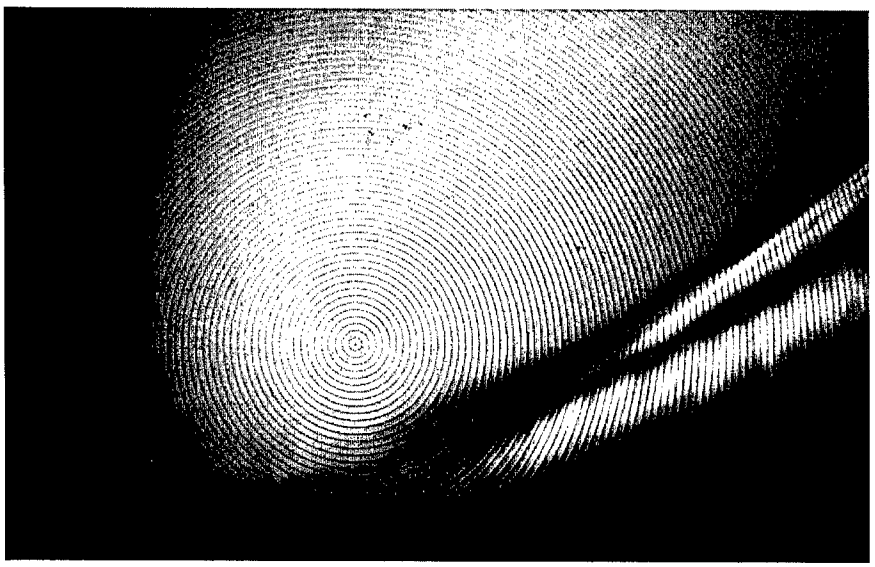

Figure 14 : SBLI, p_0=25 psi, BVC

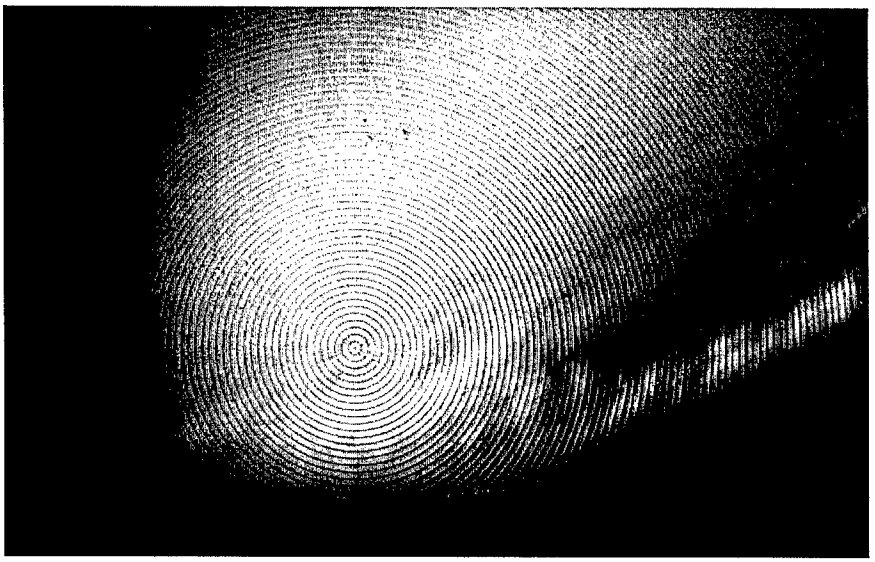

Figure 15 : SBLI, p_0=25 psi, BVO

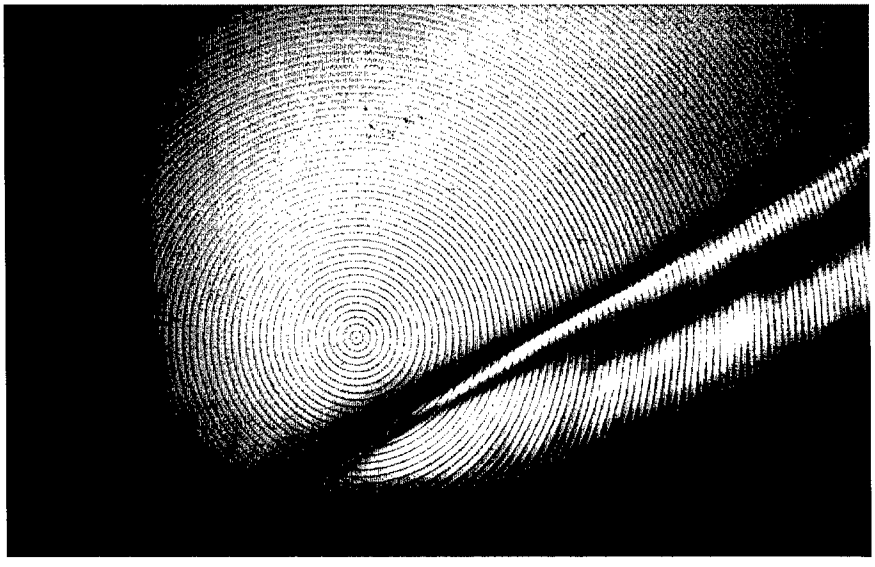

Figure 16 : SBLI, p_0=35 psi, BVC

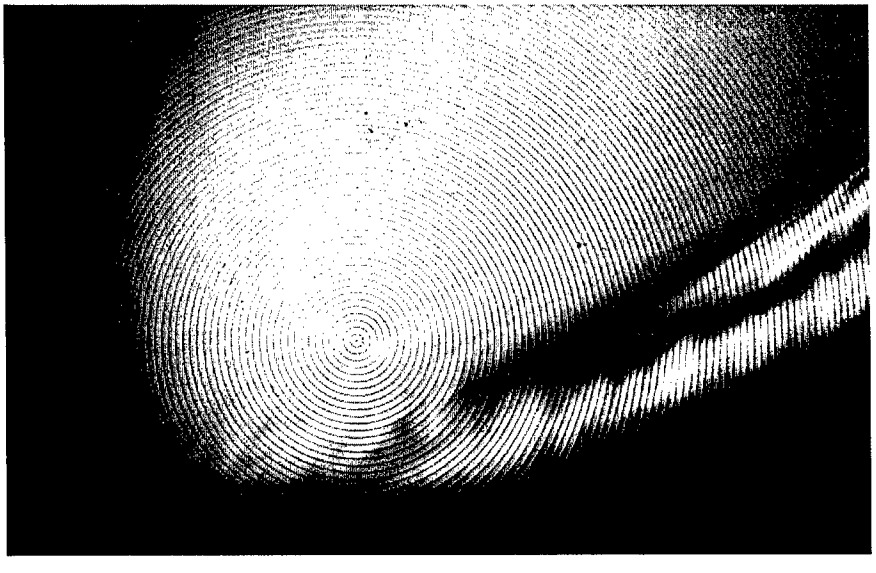

Figure 17 : SBLI, p_0=35 psi, BVO

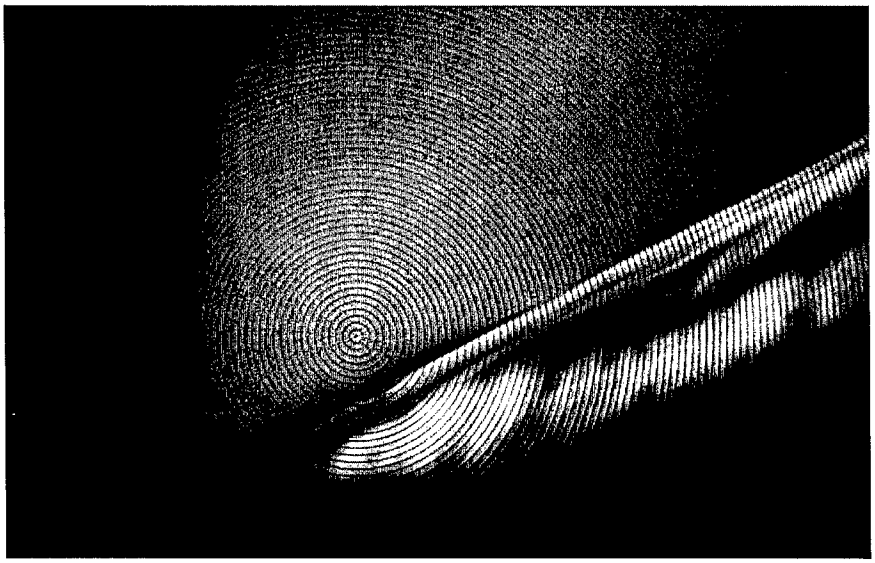

Figure 18 : SBLI, p_0=50 psi, BVC

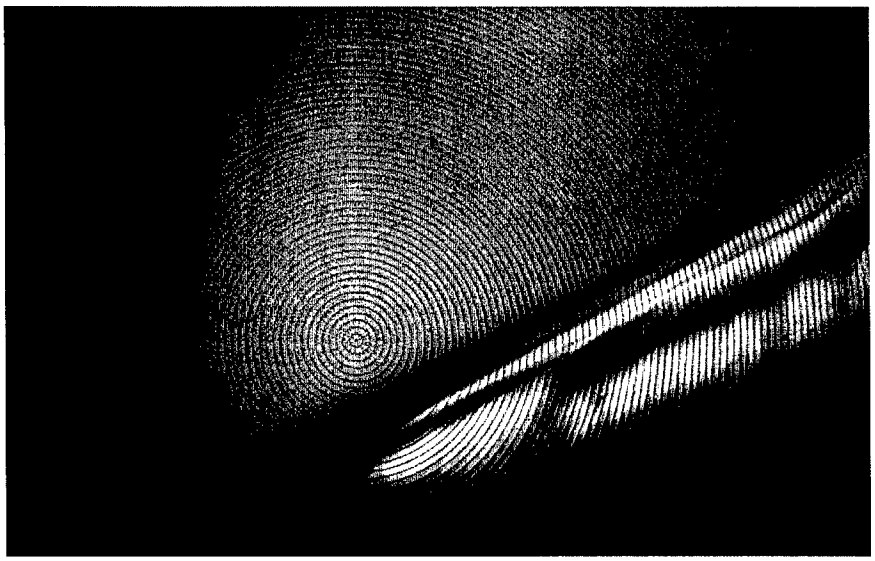

Figure 19 : SBLI, p_0=50 psi, BVO

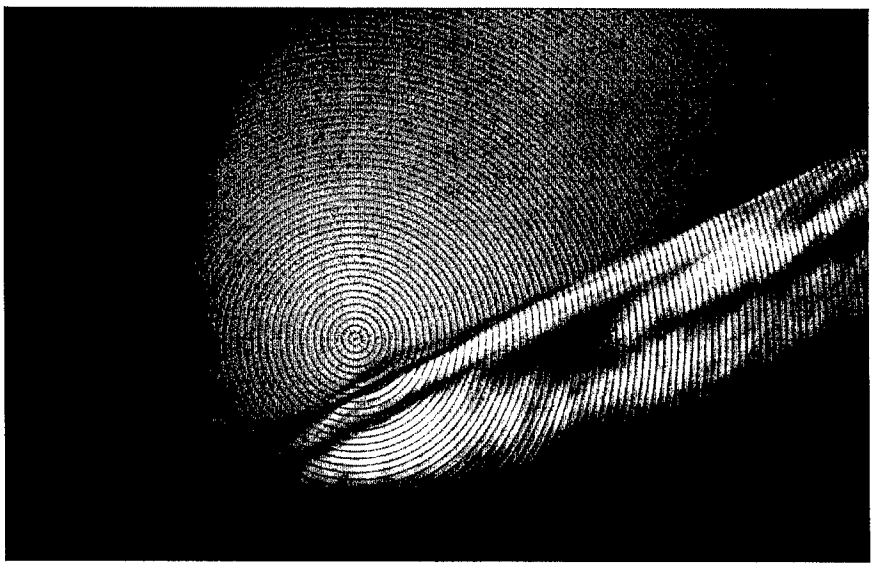

Figure 20 : SBLI, p_0=75 psi, BVC

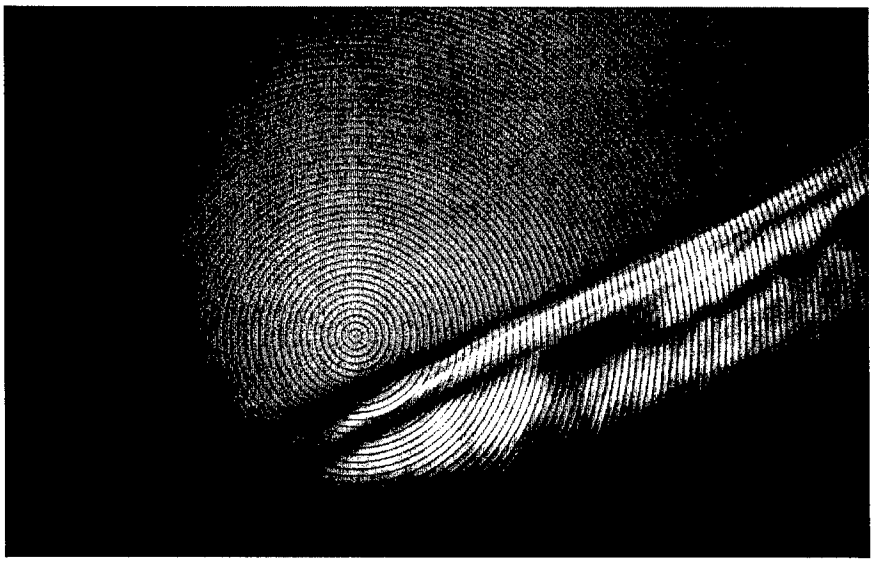

Figure 21 : SBLI, p_0=75 psi, BVO

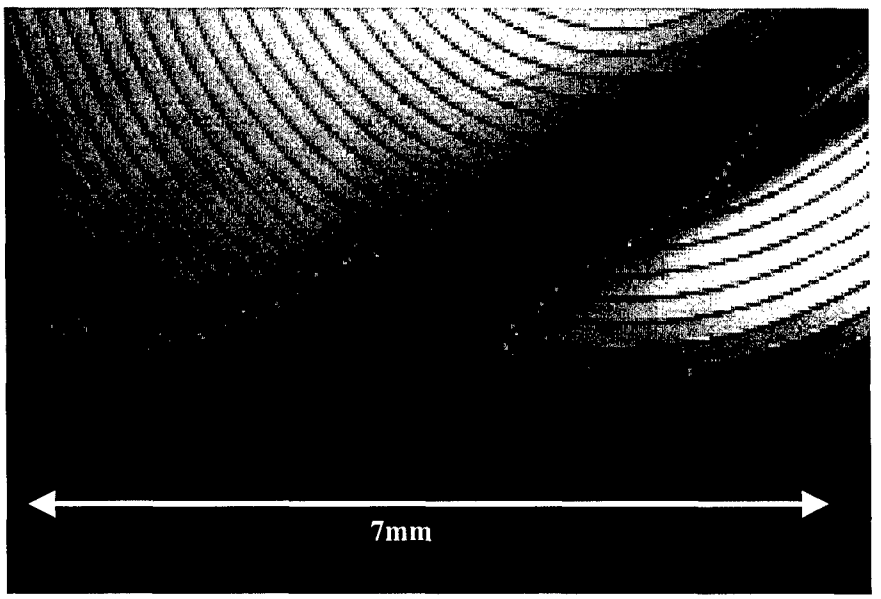

Figure 22 : zoom on shock foot, p_0=50psi, BVC